

Modeling the Anatomical Distribution of Sunlight^{¶‡}

John J. Streicher*^{†1}, William C. Culverhouse Jr.², Martin S. Dulberg² and Robert J. Fornaro²

¹National Oceanic and Atmospheric Administration, Research Triangle Park, NC and

²Department of Computer Science, North Carolina State University, Raleigh, NC

Received 8 August 2003; accepted 2 October 2003

ABSTRACT

One of the major technical challenges in calculating solar irradiance on the human form has been the complexity of the surface geometry (*i.e.* the surface-normal vis-a-vis the incident radiation). Over 80% of skin cancers occur on the face, head, neck and back of the hands. The quantification, as well as the mapping of the anatomical distribution of solar radiation on the human form, is essential if we are to study the etiology of skin cancers or cataracts or immune system suppression. Using advances in computer graphics, including high-resolution three-dimensional mathematical representations of the human form, the calculation of irradiance has been attained to subcentimeter precision. Lighting detail included partitioning of direct beam and diffuse skylight, shadowing effects and gradations of model surface illumination depending on model surface geometry and incident light angle. With the incorporation of ray-tracing and irradiance algorithms, the results are not only realistic renderings but also accurate representations of the distribution of light on the subject model. The calculation of light illumination at various receptor points across the anatomy provides information about differential radiant exposure as a function of subject posture, orientation relative to the sun and sun elevation. The integration of a geodesic sun-tracking model into the lighting module enabled simulation of specific sun exposure scenarios, with instantaneous irradiance, as well as the cumulative radiant exposure, calculated for a given latitude, date, time of day and duration. Illustration of instantaneous irradiance or cumulative radiant exposure is achieved using a false-color rendering—mapping light intensity to color—creating irradiance or exposure isopleths. This approach may find application in the determination of the reduction in

exposure that one achieves by wearing a hat, shirt or sunglasses. More fundamentally, such an analysis tool could provide improved estimates of scenario-specific dose (*i.e.* absorbed radiant exposure) needed to develop dose–response functions for sunlight-induced disease.

INTRODUCTION

Etiology

The Skin Cancer Foundation, New York, reports that over 80% of skin cancers occur on the face, head, neck and back of the hands. The epidemiological record clearly establishes solar ultraviolet radiation (UVR) as a causal agent in skin cancers; however, the dose–effect relationship is not necessarily linear nor is anatomical location of applied dose necessarily collocated with tumor induction (1–5). The dose metric (*i.e.* radiant exposure rate weighting function) applicable for induction of a given type of skin cancer may be specific to that cancer. Squamous cell carcinoma (SCC) appears to be a linear dose–effect function, with cumulative lifetime dose being predictive of SCC induction, and the anatomical site of SCC seems to be related to the lifetime cumulative sun exposure at that site (6). Kaminer (7) noted that greater than 75% of SCC in the United States occur on the sun-exposed head, neck and hands. In Caucasians, the incidence of SCC on the nose is more than 200 times the incidence on the trunk. Basal cell carcinoma (BCC) may be related to intermittent exposures (8). Thus, the dose rate appears to play a role, in addition to the cumulative absorbed exposure. Chuang *et al.* (9) reported that most of the BCC were distributed on the sun-exposed areas of the head and neck. It has been suggested that BCC frequency may be related to the location of sebaceous glands (head, trunk and shoulders). Thus, an anatomically differential susceptibility may be involved in BCC. A relationship between acute exposure (*i.e.* a childhood history of sunburn) and cutaneous malignant melanoma (CMM) was established by several investigators (10–14). Anatomical location of CMM frequency is not well correlated with exposure site (15–17). This does not imply that UVR is not a causal agent. Rather, the applicable (nonlinear) dose metric for irradiance as a function of time (including thresholds and respites) may be governed by the mechanisms involved in cellular damage, repair and transformation (18–19).

Ambient vs personal exposure

Further complicating the issue is the nonuniformity of the anatomical distribution of sun exposure, as evidenced by erythema, sunburn or nevi density. An improved understanding of skin cancer etiology depends on reducing uncertainty in the dose estimate associated with a given exposure scenario. The assessment of

¶Posted on the website on 26 October 2003.

*To whom correspondence should be addressed at: U.S. Environmental Protection Agency, Attn: Streicher, Mail Drop E243-04, Research Triangle Park, NC 27711, USA. Fax: 919-541-9420; e-mail: streicher.john@epa.gov

†On Assignment to the U.S. Environmental Protection Agency, Research Triangle Park, NC 27711.

‡The United States Environmental Protection Agency through its Office of Research and Development funded and managed the research described here under assistance agreement number R829432010 to North Carolina State University. It has been subjected to EPA and NOAA review and approved for publication.

Abbreviations: BCC, basal cell carcinoma; CMM, cutaneous malignant melanoma; 3D, three dimensional; RRT, recursive ray tracer; SCC, squamous cell carcinoma; UVR, ultraviolet radiation.

© 2004 American Society for Photobiology 0031-8655/04 \$5.00+0.00

potential human exposure to solar radiation has traditionally been equated to a horizontal-surface irradiance. The public service reporting of a UV Index is based on an erythemal weighting of the next day forecast of solar noon horizontal-surface irradiance (20). Horizontal-surface irradiance is, however, a poor surrogate for human exposure (21,22). The human form, by virtue of its complex geometry, receives highly variable sunlight irradiance across its surface area. Total irradiance incident on a surface consists of both direct and diffuse light, both of which vary with surface slope and aspect. Body surfaces most intensely illuminated are a function of sun elevation, as well as the posture and orientation of the individual. The human form's cylindrical asymmetry further requires that orientation vis-a-vis the sun's azimuth be an integral part of the exposure calculation. Posture, as a variable shape factor, must also be specified. Exposure of the eye is particularly poorly represented by a horizontal-surface irradiance because gaze is almost never toward the zenith. The experimental work of numerous researchers has sought to improve the precision of human sunlight exposure assessment by demonstrating the variability of solar irradiance across the anatomy. Such work has focused primarily on the UV portion of the solar spectrum, using polysulfone film as a detector on fixed or rotating mannequins (1, 23–29) or human subjects participating in various recreational activities (30–35). These experiments have shown that only total body burden would seem to be approximated by a horizontal-surface irradiance. Modeling human exposure to solar radiation therefore demands that exposure calculation be anatomically resolved. The accurate calculation of irradiance at various anatomical locations would provide information about differential exposure as a function of subject posture, orientation relative to the sun and sun elevation. By integrating geodesic sun-tracking models with high-resolution three-dimensional (3D) mathematical computer models of the human form, the instantaneous irradiance can be calculated, as well as the cumulative radiant exposure received during a sun exposure scenario, at selected locations on the anatomy.

Presented in this study is a proof-of-concept simulation model. The objective of the model is to quantify the radiant exposure of solar radiation that is incident on the human form during an arbitrary exposure scenario. The scenario is defined by geodesic, atmospheric and human activity variables. With the specification of location (latitude and longitude), date, time of day, exposure duration, broadband atmospheric transmissivity and subject posture, the model calculates the cumulative broadband radiant exposure at 40 anatomical regions and provides the separate attribution for both direct (beam) and diffuse (skylight) that contribute to the total incident exposure. The model output also includes a graphic rendering of the subject in either “true” color or “false” color that is used to illustrate the most- to least-exposed anatomical regions, in a continuous color gradation across the anatomy. Results for two of the more important static postures—standing and reclining with the face up (as in sun bathing)—are reported for four solar zenith angles and eight relative aspects.

Definitions

Irradiance, E , is defined as the incident flux impinging on a surface and has units of W/m^2 . Irradiance is the integral of spectral irradiance, E_{λ} , over a specified wavelength region, *e.g.* (λ_1, λ_2), where $\lambda_1 < \lambda_2$. Radiant exposure, H , is defined as the energy incident on a surface during a given time interval, (t_1, t_2), where $t_1 < t_2$.

Radiant exposure has units of J/m^2 , and is the integral of spectral radiant exposure, H_{λ} , over a specified wavelength region, *e.g.* (λ_1, λ_2), where $\lambda_1 < \lambda_2$. The term dose refers to the fraction of radiant exposure that is absorbed per unit area and depends on reflectance and absorptivity of the irradiated material. The unit of dose is J/m^2 . Biologically effective irradiance, biologically effective radiant exposure and biologically effective dose may be computed by multiplying a spectral weighting function (*i.e.* “action spectrum”) by the spectral irradiance, spectral radiant exposure and spectral dose, respectively.

MODEL DESIGN

Overview

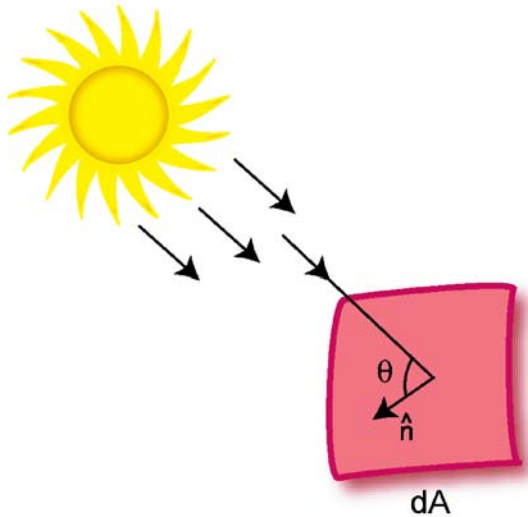
The objective of the simulation model is to quantify the energy of solar radiation that is incident on the human form during an arbitrary exposure scenario. A scenario is defined by geodesic, atmospheric and human activity variables. Specifically, the model inputs specify location (latitude and longitude), date, time of day, exposure duration, atmospheric transmissivity, activity and clothing.

The assessment of anatomically resolved irradiance and radiant exposure for short-duration (*i.e.* continuous) sun exposure scenarios required the integration of solar trajectory and radiative transfer models with 3D graphic models of the human form and ray-tracing or illumination software. The solar trajectory component calculated solar zenith and azimuth angles, given latitude, longitude, date and time of day. The radiative transfer component calculated spectrally integrated direct and diffuse irradiance onto a surface polygon of arbitrary orientation, given solar zenith and azimuth angles and the surface-normal vector's slope and aspect angles. Mathematical models of the human form with near-photographic quality surfaces were incorporated into the software, with some consisting of as many as a quarter million planar surface elements (polygons). The graphics ray-tracing component determined the surface-normal vector for all surface polygons comprising the human graphic model and determined the direct and diffuse illumination for each polygon based on relative orientation to the sun (direct light) and sky view factor (diffuse light). Identifiable anatomical features (*e.g.* the right eye), often consisting of hundreds of surface polygons, were defined by grouping appropriate polygons into a data structure for calculation of a statistical mean irradiance or numerical integration of mean irradiance over time to give mean exposure associated with the anatomical feature.

Solar trajectory model

A geodesic sun-tracking model was developed to determine sun position in the sky. This computer simulation model determined the zenith and azimuth angles of the sun, given user-specified latitude, longitude, date and time of day. Fourier series numerical algorithms were used to compute solar declination and the equation of time (36). Closed-function algorithms were used to compute the solar azimuth and zenith angles (37). An algorithm for refraction correction of zenith angle was developed using a statistical regression of observed vs astronomical values of the zenith angle. Consequently, this model accounts for atmospheric refraction because it perturbs the apparent sun zenith angle, as well as apparent sunrise and sunset times. Assignment of local standard times was based on the nearest standard meridian to the east of the simulation longitude. The calculated sun coordinates were validated

Calculation of Irradiance on Elemental Surface dA



Elemental Surface Irradiance = Normal Flux x cos θ
 Elemental Surface Exposure = \int (Surface Irradiance x dA) dt

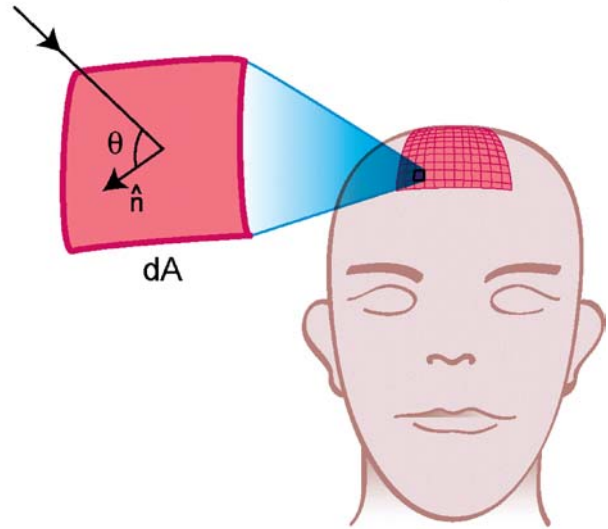
Figure 1. The surface of the 3D subject model is constructed from numerous 2D polygons. Each polygon has a well-defined orientation in space, specified by its surface normal vector \hat{n} . This orientation determines the incident angle of direct light as well as the sky view factor for diffuse light.

against published tables (38); agreement was found to be within 1° of zenith and azimuth.

Broadband radiative transfer model

An atmospheric transmission model for broadband solar radiation calculated the direct (*i.e.* beam) irradiance and diffuse sky irradiance onto surfaces of arbitrary orientation. This model accounted for the variation in extraterrestrial solar irradiance over the course of a year because of the changing earth–sun distance as the earth moves in an elliptical orbit about the sun. A Fourier series numerical algorithm was used to calculate earth–sun distance (36). The solar constant used was 1367 W/m². Broadband atmospheric transmittance was incorporated as an independent input variable, where values ranging from 0.50 (corresponding to a very hazy atmosphere) to 0.80 (very clear) would be appropriate. (A transmissivity of 0.65 would be valid for typical aerosol loading at sea level elevation). Direct irradiance was attenuated as described by Beer’s law, with the optical path length increasing approximately as the secant of the solar zenith angle. Direct irradiance onto a surface of arbitrary orientation was computed using standard spherical trigonometry formulas, given the solar zenith and azimuth angles and the slope and aspect angles of the surface (37,39, 40). Total diffuse irradiance onto a horizontal surface was calculated from normal direct irradiance based on a formulation that considered seasonal variations in water vapor (41,42). Diffuse irradiance onto a surface of arbitrary orientation was based on the Temps and Coulson (43) formulation that accounts for (1) sky view factor of the surface; (2) circumsolar diffuse radiation; and (3) near-horizon diffuse radiation. The diffuse irradiance algorithm did not incorporate ground reflectance. The partition of direct and diffuse light allowed

Anatomical "Patch" Irradiance & Exposure



Mean Patch Irradiance = $\frac{1}{N} \sum_{i=1}^N$ Elemental Surface Flux
 Patch Radiant Exposure = \int (Mean Patch Irradiance) dt

Figure 2. Anatomical region patch shown here for vertex of head. The patch is defined by numerous contiguous polygons. The mean patch irradiance is defined as the mean of the irradiances of all comprising polygons. The patch radiant exposure is defined as the time integral of the mean patch irradiance.

independent tabulation of their contribution to total irradiance and hence independent attribution of their contribution to irradiance and radiant exposure.

The 3D human graphic model

High-resolution mathematical models of the human form consist of thousands of polygons—each having a well-defined orientation in space as defined by the polygons’s surface-normal vector. The calculation of surface-direct irradiance is possible by calculating the vector dot-product between the surface-normal and the incoming light ray (Fig. 1). Calculation of the diffuse component depends on surface orientation vis-a-vis the sun position as well as the sky view factor (the fraction of the 2 π steradian view that is occupied by radiant sky vs nonsky).

Anatomical surface features (*e.g.* eye, forehead) were defined by grouping the appropriate contiguous surface polygons into data structures. This allowed a mean irradiance or mean cumulative exposure to be calculated for commonly understood and recognizable body locations (Fig. 2). Forty anatomical regions were defined for this work and are shown as patches in front view (Fig. 3a), posterior view (Fig. 3b) and close-up of the face (Fig. 3c). These anatomical regions were selected taking into consideration the published anatomical exposure measurement literature. The relative anatomical precision of irradiance and/or exposure calculations would then depend on the number of polygons comprising the model. The quality of graphical illustration of irradiance or radiant exposure would likewise be limited by polygon count. A continuous and smooth curvature of the “skin” would enable the gradations of incident light to map smoothly onto its surface for realistic true-color renderings. In this work, the graphic model chosen for study was

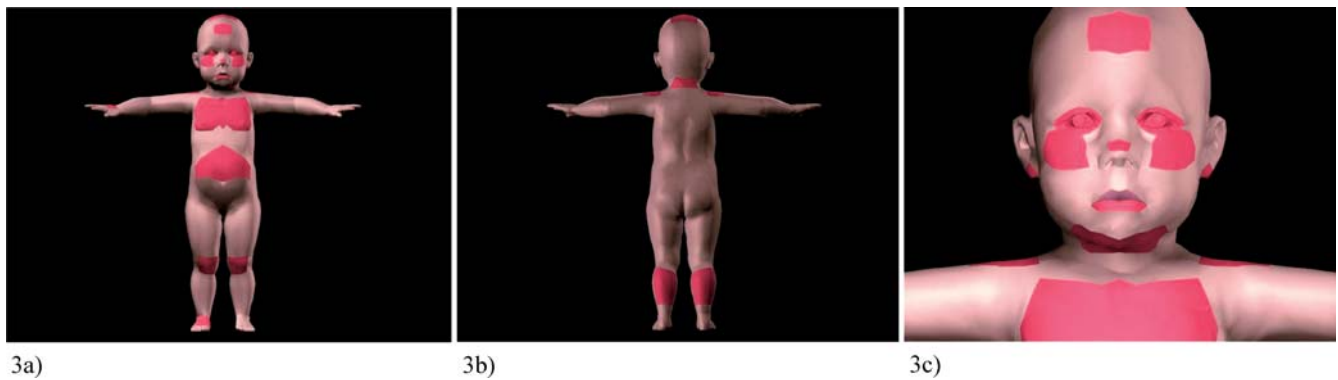


Figure 3. Subject model showing anatomical region modeling patches in red. Front view (a) displays patches on face, chest, abdominal region, knees and dorsal foot. Posterior view (b) displays patches on the vertex of the head, nape of the neck, shoulders and calves. Close-up of face (c) displays patches on forehead, eyes, cheeks, nose tip, lower lip, ear lobes and underside of chin.

a toddler known as the “Dancing Baby”[®], developed by Autodesk, Inc. (San Rafael, CA) and was used with permission.

The utility of rendering of the model was further extended to show the relative anatomical distribution of sunlight using full-spectrum false-color, where red skin indicated regions subjected to the greatest irradiance (or radiant exposure) and blue skin indicated the regions subjected to the least. Intermediate colors of the spectrum (orange, yellow, green) indicated proportionately more-to-less linear gradients.

To simulate plausible sunlight exposures incurred during a variety of outdoor scenarios, several static postures were created including standing, sitting, lying with the face up and lying with the face down. In addition, animated activities such as walking, playing and swimming were created from multiframe still model forms. Both static postures as well as dynamic activities could be simulated for either instantaneous irradiance or cumulative exposure corresponding to any latitude, longitude, date, time of day and scenario duration (for cumulative exposure cases).

Ray-tracing model

The calculation of irradiance on polygons as well as rendering the subject model for graphic output was achieved within a modified recursive ray tracer (RRT). The typical usage of RRT, where each pixel is colored based on a combination of incident (direct and diffuse) and reflected light, is limited to screen image rendering of a virtual scene by a virtual light source (44). Relative locations of light sources, subject and viewing perspective are determined using

analytic geometry in a 3D coordinate system. The lighting detail (hue, saturation, intensity) of each polygon within the virtual scene would be determined by a systematic examination of geometric rays from source-to-polygon and from polygon-to-observer. Contributions from both point sources (*e.g.* the sun) and area sources (*e.g.* diffuse sky light) would be considered (45,46). The reflectance of the polygon, in addition to incident and reflected light angle, would then determine the polygon’s observed color (hue, saturation) and brightness (intensity).

With consideration of photobiological applications, modifications to the generic RRT algorithm were made to calculate and view incident but not reflected light. In addition, because the spatial pattern of diffuse sky radiance is not isotropic, the irradiance onto an arbitrarily oriented surface must calculate not only the overall sky view factor but the view of the specific radiant sky as relative to the sun. Thus, the observed image is not a picture that would ever be seen (as by reflected light), rather it is a research graphic displaying irradiance (Fig. 4a). Anatomical regions of interest were defined as groups of contiguous polygons. Total irradiance was calculated for each polygon comprising a defined anatomical group and averaged over all polygons in the group. Values of irradiance for all defined anatomical regions were then reported. A final modification of the RRT allowed an optional false-color rendering of the scene, using polygon-specific irradiance values (calculated during a first pass) to render polygon color according to an irradiance-to-color mapping function. The scene observed in false color illustrates the incident light pattern so explicitly as to delineate irradiance (or radiant exposure) isopleths (Fig. 4b).

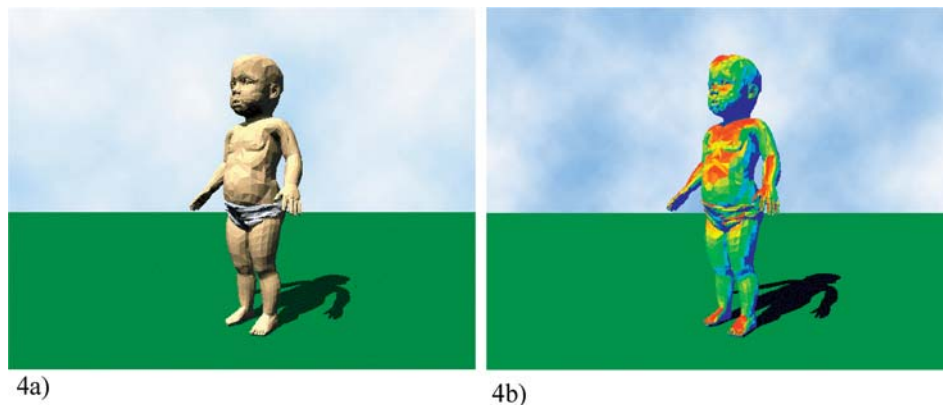


Figure 4. Subject model showing irradiance (direct plus diffuse) across the anatomy in true color (a) and in false color (b). False-color rendering—mapping irradiance magnitude to a color spectrum—demonstrably illustrates the gradation of sunlight irradiance across the anatomy, with red indicating the areas of greatest irradiance, scaling down through orange, yellow, green and blue.

Table 1. Irradiance ratios for standing posture at 10° solar elevation

Anatomical region	(Subject aspect – solar azimuth)				
	0°	45°	90°	135°	180°
Head vertex	0.92	0.97	1.17	1.35	1.33
Forehead	3.93	2.91	0.80	0.30	0.30
Nose tip	3.22	2.46	1.40	0.31	0.31
Cheek (L/R)	3.20	3.95/1.06	2.55/0.27	0.51/0.27	0.27
Lower lip	3.15	2.40	1.04	0.26	0.26
Ear lobe (L/R)	1.22	2.43/0.16	2.27/0.16	0.91/0.16	0.20
Nape of neck	0.25	0.25	0.74	2.69	3.73
Shoulder top (L/R)	0.86	1.43/0.46	2.19/0.34	2.25/0.69	1.60
Upper back	0.23	0.23	0.36	2.67	3.76
Chest (L/R)	3.58	3.40/2.70	1.53/0.96	0.28/0.28	0.28
Thigh front (L/R)	3.75	2.58/2.78	0.65/0.27	0.23/0.23	0.23
Calf (L/R)	0.25	0.33/0.37	1.18/0.39	2.37/2.49	3.16
Dorsal foot (L/R)	2.58	2.43/1.97	1.46/0.95	0.59/0.56	0.34

Model validation

Verification of the internal accuracy of both irradiance and radiant exposure calculation was accomplished by using a geometric cube as the illumination subject. The procedural steps in running an illumination scenario for the cube graphic were identical to those for the human graphic. The coordinate orientation of the cube was aligned so that cube faces were parallel with cartographic lines in the coordinate system of the integrated model. The integrated modeling system (solar trajectory, radiative transfer, 3D cube and ray tracer) was then run for various scenarios of latitude, longitude, date, time and duration. The six faces of the cube had known slope and aspect, and thus the irradiance or radiant exposure (or both)—for direct and diffuse independently—was checked against and verified to agree with calculations from a stand-alone program incorporating the geodesic and radiative transfer algorithms run for vertical surfaces facing east, west, north and south, as well as a horizontal surface.

RESULTS

Presented here are irradiance ratios calculated at 20 anatomical locations for two static postures: a standing posture (Tables 1–4) and a prone face-up posture (Tables 5–8). Presenting irradiance as irradiance ratios (anatomical site irradiance divided by horizontal-

Table 2. Irradiance ratios for standing posture at 25° solar elevation

Anatomical region	(Subject aspect – solar azimuth)				
	0°	45°	90°	135°	180°
Head vertex	0.78	0.82	0.94	1.05	1.09
Forehead	2.07	1.59	0.52	0.15	0.15
Nose tip	1.81	1.45	0.81	0.16	0.16
Cheek (L/R)	1.61	1.96/0.61	1.31/0.14	0.27/0.14	0.14
Lower lip	1.54	1.19	0.49	0.13	0.13
Ear lobe (L/R)	0.48	1.04/0.08	0.97/0.08	0.35/0.08	0.08
Nape of neck	0.13	0.13	0.37	1.29	1.78
Shoulder top (L/R)	0.68	1.10/0.19	1.48/0.18	1.50/0.63	1.13
Upper back	0.12	0.12	0.18	1.20	1.71
Chest (L/R)	1.81	1.73/1.40	0.84/0.55	0.15/0.14	0.14
Thigh front (L/R)	1.72	1.18/1.27	0.25/0.12	0.12/0.12	0.12
Calf (L/R)	0.13	0.17/0.15	0.57/0.30	1.13/1.18	1.50
Dorsal foot (L/R)	1.61	1.52/1.30	1.04/0.67	0.43/0.30	0.18

Table 3. Irradiance ratios for standing posture at 45° solar elevation

Anatomical region	(Subject aspect – solar azimuth)				
	0°	45°	90°	135°	180°
Head vertex	0.84	0.87	0.92	0.98	1.00
Forehead	1.22	0.99	0.46	0.12	0.10
Nose tip	1.17	0.99	0.59	0.11	0.10
Cheek (L/R)	0.91	1.07/0.42	0.76/0.09	0.18/0.09	0.09
Lower lip	0.84	0.55	0.22	0.09	0.08
Ear lobe (L/R)	0.17	0.43/0.05	0.39/0.05	0.14/0.05	0.05
Nape of neck	0.08	0.08	0.18	0.67	0.91
Shoulder top (L/R)	0.71	0.96/0.12	1.15/0.12	1.16/0.43	0.98
Upper back	0.07	0.07	0.13	0.56	0.80
Chest (L/R)	1.00	0.98/0.79	0.55/0.37	0.13/0.11	0.09
Thigh front (L/R)	0.83	0.56/0.61	0.08/0.08	0.08/0.08	0.08
Calf (L/R)	0.08	0.11/0.08	0.31/0.26	0.59/0.61	0.76
Dorsal foot (L/R)	1.17	1.11/1.00	0.87/0.58	0.48/0.29	0.11

surface irradiance) effectively normalizes the variability of cloudless sky broadband atmospheric transmissivity. Calculation of diffuse irradiance from ground reflection is neglected by assigning an albedo of zero to all surfaces—ground and subject. Because these data present a spectrally integrated irradiance (*i.e.* total solar spectrum), they are not directly comparable with experimental work that has measured erythemally weighted UV-B. Rayleigh scattering is strongly wavelength dependent, and hence the relative contribution of direct and diffuse irradiance onto an arbitrarily oriented surface will be wavelength dependent. In all irradiance calculations, total irradiance was determined as the sum of direct and sky diffuse irradiance.

Each posture is irradiated under four solar elevations (10°, 25°, 45° and 65°) and five relative aspects (0°, 45°, 90°, 135° and 180°). The relative aspect is defined as the subject’s aspect minus the solar azimuth. The aspect of a subject in standing posture is defined as the direction faced; the aspect of a subject in prone face-up posture is defined as the direction vector originating at the subject’s head and terminating at the subject’s feet (*e.g.* prone subject with a north-south alignment, having head at north end and feet at south end, would have aspect of 180°). The subject’s bilateral symmetry may be exploited to determine the full 360° of relative aspect for any anatomical region having a left and right component.

Table 4. Irradiance ratios for standing posture at 65° solar elevation

Anatomical region	(Subject aspect – solar azimuth)				
	0°	45°	90°	135°	180°
Head vertex	0.88	0.89	0.92	0.95	0.96
Forehead	0.81	0.70	0.45	0.22	0.16
Nose tip	0.86	0.77	0.57	0.09	0.09
Cheek (L/R)	0.56	0.64/0.28	0.49/0.07	0.12/0.07	0.07
Lower lip	0.27	0.19	0.11	0.07	0.07
Ear lobe (L/R)	0.09	0.18/0.04	0.15/0.04	0.04/0.04	0.04
Nape of neck	0.07	0.07	0.07	0.10	0.12
Shoulder top (L/R)	0.75	0.90/0.12	0.98/0.10	0.99/0.21	0.90
Upper back	0.06	0.06	0.09	0.27	0.37
Chest (L/R)	0.55	0.57/0.43	0.38/0.23	0.19/0.13	0.07
Thigh front (L/R)	0.38	0.26/0.08	0.10/0.06	0.06/0.06	0.06
Calf (L/R)	0.07	0.07/0.07	0.20/0.07	0.33/0.34	0.40
Dorsal foot (L/R)	0.95	0.91/0.87	0.76/0.09	0.46/0.18	0.09

Table 5. Irradiance ratios for prone posture (face-up) at 10° solar elevation

Anatomical region	(Subject aspect – solar azimuth)				
	0°	45°	90°	135°	180°
Head vertex	0.23	0.23	0.68	2.63	3.68
Forehead	0.36	0.68	1.46	1.99	2.33
Nose tip	0.32	0.53	1.37	2.26	2.73
Cheek (L/R)	0.41	1.63/0.36	2.65/0.55	2.57/0.81	1.09
Lower lip	0.93	1.17	1.49	1.12	0.42
Ear lobe (L/R)	0.35	2.76/0.32	2.40/0.28	1.24/0.27	0.28
Underside chin	0.73	2.10	1.02	0.28	0.28
Shoulder top (L/R)	0.21	0.24/0.21	1.36/0.23	3.17/0.25	2.54
Chest (L/R)	0.35	1.19/0.37	1.97/0.56	2.22/0.88	1.24
Abdomen	1.05	1.15	1.24	1.15	1.04
Thigh front (L/R)	1.29	1.19/1.37	1.14/1.35	0.88/0.69	0.46
Dorsal foot (L/R)	0.36	0.38/0.53	2.25/0.64	3.21/1.03	1.69
Sole foot (L/R)	2.88	2.06/2.06	0.38/0.23	0.22/0.17	0.17

Although the largest irradiance ratios are to be expected on surfaces with a normal orientation to the sun during low sun elevations (Tables 1, 2, 5 and 6), the absolute irradiance will be greatly attenuated by the long optical path length through the atmosphere. Sensitive regions (*e.g.* eyes) or rarely exposed regions (*e.g.* soles of feet) may receive injury nonetheless. Of greater importance are the irradiances on anatomical regions having near-normal orientations to the sun for sun elevations greater than 45°. Tables 3 and 4 indicate that a standing posture preferentially exposes the face, head, shoulders and dorsal area of the foot (ratios > 1), depending on relative aspect. Tables 7 and 8 indicate that a prone face-up posture preferentially exposes the face, chest, abdomen and thighs. Somewhat counterintuitive are certain anatomical regions that are maximally exposed for relative aspects other than 0° (vertex of head at 180°, standing and prone; shoulder at 135°, standing and prone). Thus “sun-averting” direction—typically taken to mean a relative aspect of 180°—equates to “sun-seeking” for some anatomical regions.

DISCUSSION

Quantifying incident solar energy by anatomical location for arbitrary exposure scenarios is essential if we are to gain under-

Table 6. Irradiance ratios for prone posture (face-up) at 25° solar elevation

Anatomical region	(Subject aspect – solar azimuth)				
	0°	45°	90°	135°	180°
Head vertex	0.12	0.12	0.34	1.22	1.70
Forehead	0.27	0.53	0.94	1.30	1.50
Nose tip	0.17	0.35	0.91	1.34	1.60
Cheek (L/R)	0.38	1.06/0.34	1.57/0.46	1.56/0.60	1.01
Lower lip	0.70	0.79	0.94	0.88	0.47
Ear lobe (L/R)	0.74	1.45/0.17	1.28/0.15	0.75/0.14	0.25
Underside chin	1.48	1.34	0.56	0.14	0.14
Shoulder top (L/R)	0.11	0.12/0.11	0.58/0.13	1.41/0.12	1.08
Chest (L/R)	0.50	0.93/0.39	1.35/0.56	1.49/0.82	1.11
Abdomen	0.90	0.93	0.97	0.96	0.94
Thigh front (L/R)	1.11	1.02/1.11	0.89/1.02	0.79/0.87	0.76
Dorsal foot (L/R)	0.23	0.41/0.32	1.35/0.40	1.81/0.83	1.58
Sole foot (L/R)	1.17	0.77/0.83	0.13/0.12	0.09/0.09	0.09

Table 7. Irradiance ratios for prone posture (face-up) at 45° solar elevation

Anatomical region	(Subject aspect – solar azimuth)				
	0°	45°	90°	135°	180°
Head vertex	0.08	0.08	0.20	0.59	0.83
Forehead	0.40	0.53	0.77	1.01	1.12
Nose tip	0.23	0.40	0.71	0.95	1.09
Cheek (L/R)	0.50	0.85/0.41	1.10/0.46	1.09/0.57	0.84
Lower lip	0.63	0.68	0.77	0.77	0.74
Ear lobe (L/R)	0.64	0.87/0.34	0.79/0.09	0.54/0.12	0.25
Underside chin	1.00	0.81	0.39	0.12	0.09
Shoulder top (L/R)	0.07	0.08/0.07	0.27/0.10	0.64/0.21	0.53
Chest (L/R)	0.64	0.87/0.55	1.08/0.63	1.16/0.82	1.04
Abdomen	0.88	0.88	0.90	0.91	0.91
Thigh front (L/R)	1.02	0.97/1.02	0.91/0.97	0.86/0.91	0.86
Dorsal foot (L/R)	0.26	0.54/0.27	0.95/0.39	1.18/0.73	1.08
Sole foot (L/R)	0.44	0.23/0.29	0.06/0.07	0.06/0.06	0.06

standing into the process of tissue and immune system damage associated with specific activities. Extrapolating the measured threshold exposures for induction of observable changes in laboratory animals to human subjects requires not only the extrapolation across species but also in equating controlled exposures to plausible human activity scenarios.

The proof-of-concept simulation model reported in this study has incorporated several environmental and human activity simplifications, each of which will be addressed in future model development. The environmental simplifications have included a spectrally integrated radiative transfer component that calculates incident broadband (total solar spectrum) irradiance. The direct-to-diffuse ratios for UVR are somewhat different from those for broadband, as is the pattern of diffuse sky radiance. The degree to which the total solar spectrum is an adequate surrogate for UVR will be examined in a future study. Second, only cloudless sky conditions are modeled, nevertheless a range of aerosol loadings may be achieved by modifying the transmissivity. Finally, reflected radiation is neglected. For dark surfaces, this is acceptable, but it is anticipated that surfaces such as snow would contribute significant reflected radiation. The human activity simplifications reported here have limited “activities” to static postures. Dynamic activities (*e.g.* walking) are complex choreographs consisting of sequences of

Table 8. Irradiance ratios for prone posture (face-up) at 65° solar elevation

Anatomical region	(Subject aspect – solar azimuth)				
	0°	45°	90°	135°	180°
Head vertex	0.06	0.08	0.15	0.30	0.40
Forehead	0.58	0.63	0.76	0.88	0.93
Nose tip	0.38	0.47	0.61	0.77	0.83
Cheek (L/R)	0.58	0.75/0.48	0.87/0.50	0.86/0.61	0.75
Lower lip	0.65	0.67	0.71	0.73	0.73
Ear lobe (L/R)	0.41	0.45/0.33	0.52/0.26	0.36/0.25	0.29
Underside chin	0.63	0.53	0.32	0.16	0.12
Shoulder top (L/R)	0.06	0.07/0.06	0.17/0.10	0.30/0.18	0.31
Chest (L/R)	0.74	0.85/0.69	0.95/0.72	0.99/0.82	0.93
Abdomen	0.88	0.89	0.89	0.90	0.90
Thigh front (L/R)	0.98	0.96/0.98	0.92/0.96	0.90/0.92	0.90
Dorsal foot (L/R)	0.44	0.59/0.41	0.78/0.50	0.89/0.67	0.84
Sole foot (L/R)	0.11	0.05/0.07	0.04/0.05	0.04/0.04	0.04

static postures. Last, clothing and sunscreen application significantly reduce exposure of the skin and must be considered in future model enhancements.

Modeling the distribution of a population's chronic sunlight exposure involves population activity data. Traditional human activity diaries lack sufficient detail concerning sun exposure. Time logged as "outdoors" does not provide information on cloud cover, clothing worn, sunscreen use or practices such as sun-seeking or sun-averting behavior. Hence, the assessment of chronic (*i.e.* annual average or cumulative lifetime) population exposure necessarily leads to the vagaries of population cohort definition, time-in-activity behavior sequences and microenvironmental radiation load. These challenges notwithstanding, reducing the uncertainty of anatomically resolved exposure associated with short-duration activities is constructive.

SUMMARY

Horizontal-surface irradiance depends on earth-sun distance, solar elevation angle and atmospheric transmissivity. It is a standard and readily available radiation measurement. However, it is a poor representation for the irradiance of any anatomical region, given the complex geometry of the human form and the dynamic postures and relative aspects exhibited during outdoor activity. Clothing, sunscreen and sun-averting or sun-seeking behavior further complicate estimates of sunlight exposure even during short-duration (continuous) exposure scenarios.

Proof of concept has been completed for a graphical analysis-based solar radiation exposure model. The 3D graphics modeling software is used to display a near-photographic quality human model and illuminate the model with a simulated sun light source. The research goals of the modeling are to develop photobiology tools that enable quantification and anatomical resolution of radiant exposure from sunlight for scenarios of varying posture and duration.

Because health effects are correlated with dose, assessing scenario-specific exposure accurately is essential for understanding disease etiology. Because induction of specific sunlight-induced diseases is dose rate dependent, application of appropriate dose metrics is likewise important in predicting one outcome for an acute dose scenario (*i.e.* sunburn) and another for a chronic dose scenario. Research into appropriate algorithms governing the time integration of irradiance (*i.e.* exposure rate weighting metrics) demands that estimates of cumulative irradiance—*i.e.* exposure—have both the accuracy and precision on the scale of anatomical features.

Acknowledgements—We thank the students of the Computer Science Department Senior Design Center at North Carolina State University for numerous contributions to the ray-tracing program. Illustrations drawn in Figs. 1 and 2 were courtesy of Aimée Streicher. Funding for this work was made possible through the efforts of Linda Porter and Denice Shaw.

REFERENCES

- Urbach, F. (1969) Geographic pathology of skin cancer. In *The Biologic Effects of Ultraviolet Radiation (with Emphasis on the Skin)* (Edited by F. Urbach), pp. 635–650. Pergamon Press, Oxford, UK.
- Brodtkin, R. H., A. W. Kopf and R. Andrade (1969) Basal-cell epithelioma and elastosis: A comparison of distribution. In *The Biologic Effects of Ultraviolet Radiation (with Emphasis on the Skin)* (Edited by F. Urbach), pp. 581–618. Pergamon Press, Oxford, UK.
- Pearl, D. K. and E. L. Scott (1986) The anatomical distribution of skin cancers. *Int. J. Epidemiol.* **15**, 502–506.
- de Gruijl, F. R. and J. C. Van der Luen (1993) Influence of ozone depletion on the incidence of skin cancer: Quantitative prediction. In *Environmental UV Photobiology* (Edited by A. R. Young, L. O. Bjorn, J. Moan and W. Nultsch), pp. 89–109. Plenum Press, New York.
- Kricker, A., B. K. Armstrong and D. R. English (1994) Sun exposure and non-melanoma skin cancer. *Cancer Causes Control* **5**, 367–392.
- Strickland, P. T., B. Vitasa, S. West, F. Rosenthal, E. Emmett and H. Taylor (1989) Quantitative carcinogenesis in man: solar ultraviolet B dose dependence of skin cancer in Maryland watermen. *J. Natl. Cancer Inst.* **24**, 1910–1913.
- Kaminer, M. S. (1995) Photodamage: Magnitude of the problem. In *Photodamage* (Edited by B. Gilchrest), pp. 1–11. Blackwell Science, Cambridge, MA.
- Gallagher, R. P., G. B. Hill, C. D. Bajdik and S. Fincham (1995) Sunlight exposure, pigmentary factors, and risk on nonmelanocytic skin cancer: I. basal cell carcinoma. *Arch. Dermatol.* **131**, 157–163.
- Chuang, T. Y., A. Popescu and W. P. Su (1990) Basal cell carcinoma: a population-based incidence study in Rochester, MN. *J. Am. Acad. Dermatol.* **22**, 413–417.
- Elwood, J. M., R. P. Gallagher, J. Davison and G. B. Hill (1985) Sunburn, suntan, and the risk of cutaneous malignant melanoma—the Western Canada Melanoma Study. *Br. J. Cancer* **51**, 543–549.
- Scotto, J. and T. R. Fears (1987) The association of solar ultraviolet and skin melanoma incidence among Caucasians in the United States. *Cancer Investig.* **5**, 275–283.
- Koh, H. K., B. E. Kligler and R. A. Lew (1990) Sunlight and cutaneous malignant melanoma: evidence for and against causation. *Photochem. Photobiol.* **51**, 765–779.
- Elwood, J. M. and B. L. Diffey (1993) A consideration of ambient solar ultraviolet radiation in the interpretation of studies of the aetiology of melanoma. *Melanoma Res.* **3**, 113–122.
- Ley, R. D. (2001) Environmental and molecular factors controlling human melanoma. In *Photobiology for the 21st Century* (Edited by T. Coohill and D. Valenzano), pp. 221–229. Valdenmar Publishing, Overland Park, KS.
- Elwood, J. M. and R. P. Gallagher (1983) Site distribution of malignant melanoma. *Can. Med. Assoc. J.* **128**, 1400–1404.
- Gallagher, R. P., D. I. McLean, C. P. Yang and A. J. Coldman (1990) Anatomic distribution of acquired melanocytic nevi in white children: a comparison with melanoma—the Vancouver mole study. *Arch. Dermatol.* **125**, 466–471.
- Rieger, E., H. P. Soyer and C. Garbe (1995) Overall and site-specific risk of malignant melanoma associated with nevus counts at different body sites: a multi center case-control study of the German Central Malignant Melanoma Registry. *Int. J. Cancer* **62**, 393–397.
- Elwood, J. M., R. P. Gallagher, G. B. Hill and J. C. G. Pearson (1985) Cutaneous melanoma in relation to intermittent and constant sun exposure—the Western Canada Melanoma Study. *Int. J. Cancer* **35**, 427–433.
- Cattaruzza, M. S. (2000) The relationship between melanoma and continuous or intermittent exposure to UV radiation. *Arch. Dermatol.* **136**, 773–774.
- Long, C. S., A. J. Miller, H. Lee, J. D. Wild, R. C. Przywarty and D. Hufford (1996) Ultraviolet index forecasts issued by the National Weather Service. *Bull. Am. Meteorol. Soc.* **77**, 729–748.
- McKenzie, R. L., K. J. Paulin and M. Kotkamp. Erythral UV irradiance at Lauder, New Zealand: relationship between horizontal and normal incidence. *Photochem. Photobiol.* **66**, 683–689.
- Parisi, A. V. and M. G. Kimlin (1999) Horizontal and sun-normal spectral biologically effective ultraviolet irradiances. *J. Photochem. Photobiol. B: Biol.* **53**, 70–74.
- Diffey, B. L., M. Kerwin and A. Davis (1977) The anatomical distribution of sunlight. *Br. J. Dermatol.* **97**, 407–410.
- Diffey, B. L., T. J. Tate and A. Davis (1979) Solar dosimetry of the face: the relationship of natural ultraviolet radiation exposure to basal cell carcinoma localization. *Phys. Med. Biol.* **24**, 931–939.
- Rosenthal, F. S., M. Safran and H. Taylor (1985) The ocular dose of ultraviolet radiation from sunlight exposure. *Photochem. Photobiol.* **42**, 163–171.
- Sliney, D. H. (1994) Epidemiological studies of sunlight and cataract: the critical factor of ultraviolet exposure geometry. *Ophthalm. Epidemiol.* **1**, 107–119.

27. Kimlin, M. G., A. V. Parisi and J. C. F. Wong (1998) The facial distribution of erythral ultraviolet exposure in south-east Queensland. *Phys. Med. Biol.* **43**, 231–240.
28. Downs, N. J., M. G. Kimlin, A. V. Parisi and J. J. McGrath (2000) Modelling human facial UV exposure. *Radiat. Prot. Aust.* **17**, 103–109.
29. Parisi, A. V., M. G. Kimlin, R. Lester and D. Turnbull (2003) Lower body anatomical distribution of solar ultraviolet radiation on the human form in standing and sitting postures. *J. Photochem. Photobiol. B: Biol.* **69**, 1–6.
30. Holman, C. D. J., I. M. Gibson, M. Stephenson and A. B. K. Armstrong (1983) Ultraviolet irradiation of human body sites in relation to occupation and outdoor activity: field studies using personal UVR dosimeters. *Clin. Exp. Dermatol.* **8**, 269–277.
31. Herlihy, E., P. H. Gies, C. R. Roy and M. Jones (1994) Personal dosimetry of solar ultraviolet radiation for different outdoor activities. *Photochem. Photobiol.* **60**, 288–294.
32. Airey, D. K., J. C. F. Wong and R. A. Fleming (1995) A comparison of human- and headform-based measurements of solar UVB dose. *Photodermatol. Photoimmunol. Photomed.* **11**, 155–158.
33. Duncan, D. D., W. Schneider, K. J. West, S. J. Kirkpatrick and S. K. West (1995) The development of personal dosimeters for use in the visible and ultraviolet wavelength regions. *Photochem. Photobiol.* **62**, 94–100.
34. Sydenham, M. M., M. J. Collins and L. W. Hirst (1997) Measurement of ultraviolet radiation at the surface of the eye. *Investig. Ophthalmol. Vis. Sci.* **38**, 1485–1492.
35. Thieden E., M. S. Ågren and H. C. Wulf. (2000) The wrist is a reliable body site for personal dosimetry of ultraviolet radiation. *Photodermatol. Photoimmunol. Photomed.* **16**, 57–61.
36. Spencer, J. W. (1971) Fourier series representation of the position of the Sun. *Search* **2**, 172.
37. Iqbal, M. (1983) *An Introduction to Solar Radiation*. Academic Press Canada, Don Mills, Canada.
38. List, R. J. (1971) *Smithsonian Meteorological Tables*. Smithsonian Institution Press, Washington, DC.
39. Ma, C. C. Y. and M. Iqbal (1983) Statistical comparison of models for estimating solar radiation on inclined surfaces. *Sol. Energy* **31**, 313–317.
40. Smart, W. M. (1977) *Textbook on Spherical Astronomy*. Cambridge University Press, Cambridge, UK.
41. Threlkeld, J. L. (1963) Solar irradiation of surfaces on clear days. *ASHRAE Trans.* **69**, 24–36.
42. Steven, M. D. (1977) Standard distribution of clear sky radiance. *Q. J. R. Meteorol. Soc.* **103**, 457–465.
43. Temps, R. C. and K. L. Coulson (1977) Solar radiation incident upon slopes of different orientations. *Sol. Energy* **19**, 179–184.
44. Glassner, A. S. (1989) *An Introduction to Ray Tracing*. Academic Press Inc., San Diego, CA.
45. Farber, E. A. and C. A. Morrison (1977) *Clear Day Design Values (ASHRAE GRP. 170)*. ASHRAE, New York.
46. Illumination Engineering Society of North America (1984) *Calculation of Daylight Availability (IES RP-21)*. IES, New York.